Research Article

Ying Yu, Ben Li*, Yu Zhang, and Chen Zhang

Deterioration characteristics of recycled aggregate concrete subjected to coupling effect with salt and frost

https://doi.org/10.1515/rams-2021-0087
received October 08, 2021; accepted November 23, 2021

Abstract: In this study, the comprehensive performance and material properties of recycled aggregate concrete (RAC) under the coupled effect of salt-frost cycles were investigated to simulate the effect of complex environmental effects on the durability and deterioration of RAC. The tests on mass loss, relative dynamic modulus of elasticity (RDME), and compressive strength of RAC were conducted after 0, 25, 50, 75, and 100 standard salt-frost cycles. The results show that the mass loss, RDME, and compressive strength of RAC develop in a bad direction with the increase of the number of salt-frost cycles and the amount of recycled aggregate admixture. The concrete damage is particularly severe at more than 40% recycled aggregate admixture. This phenomenon is explained by the changes in the microscopic morphology, distribution of the pore structure, and functional groups of RAC.

Keywords: salt-frost cycles, recycled aggregate concrete, comprehensive properties, material properties

1 Introduction

As an indispensable building material, concrete plays a pivotal role in the development of the construction industry [1,2]. However, with the continuous expansion of urbanization and rural urbanization in China, a large amount of natural resources such as sand and gravel are becoming depleted [3]. Meanwhile, the total amount of construction waste generated from the demolition of abandoned houses, road renovation, and major natural disasters is about 1.85 billion tons per year, accounting for 80–90% of the total urban waste, but the utilization rate is less than 10% [4–8]. This set of problems is causing the conventional concrete industry to struggle [9–11]. To compensate for the lack of sustainability potential of conventional concrete, an increasing amount of construction waste is being used to produce recycled aggregates, including recycled fine aggregate (FA) and recycled coarse aggregate (RCA). In addition, recycled aggregates can be used to prepare recycled aggregate concrete (RAC) by replacing natural aggregates in concrete [12,13]. At this stage, many researchers are using recycled aggregates to replace some of the natural aggregates in concrete pavements, road construction, and other civil engineering applications. They found that the low dose of recycled aggregates can make the structure with better mechanical properties and durability performance. However, the modification of recycled aggregates by dipping and adding nanomaterials allows recycled aggregates to achieve the same effect as natural aggregates [14–16]. Compared with the traditional aggregates, the application of recycled aggregates has more economic and environmental benefits.

Simultaneously, the architectural structure of the salt lake area and coastal ports in northern China has been in a complex service environment coupled with salt erosion and freezing and thawing for a long time. Buildings often suffer severe damage before reaching their normal service life. The harsh environmental conditions in the northern China pose severe challenges to the normal service of RAC. The research results on the resistance of recycled aggregates to salt-frost coupling erosion have shown that (1) The mechanical and durability performance of RAC is generally lower than that of natural aggregate concrete and decreases with the increase of RCA substitution rate [17–27]. (2) As the replacement rate of recycled aggregates increases, the frost resistance and chloride ion

* **Corresponding author: Ben Li,** Advanced and Sustainable Infrastructure Materials Group, School of Transportation and Civil Architecture, Foshan University, Foshan 528000, China, e-mail: Liben89@fosu.edu.cn
Ying Yu, Yu Zhang, Chen Zhang: Advanced and Sustainable Infrastructure Materials Group, School of Transportation and Civil Architecture, Foshan University, Foshan 528000, China

corrosion resistance of concrete decrease [28–30]. (3) The performance of recycled concrete with the same replacement rate in salt solution is worse than that in water freezing. This can be attributed to the complex microstructures in the old cement mortar adhering to the surface of the RAC, such as aggregate cracks and voids [30]. In summary, the current research on the durability of RAC under severe service environment mainly focuses on the degradation performance of recycled aggregate in a single environment. Research on related degradation characteristics under coupled conditions is insufficient, and the lack of relevant research hinders recycled aggregate. The lack of relevant studies hinders the development of regenerated aggregates and the application of concrete in cold, high latitude coastal or salt lake areas.

Therefore, it is necessary to investigate the deterioration characteristics of recycled concrete under the coupling effect of chloride salt and freeze–thaw cycles. The purpose of this study is to investigate the effects of salt-frost cycles on the surface damage, mass loss rate (MLR), relative dynamic modulus of elasticity (RDME), and cubic compressive strength of RAC with different RCA substitution rates. At the same time, the internal microscopic damage of the recycled concrete after salt-frost cycles is investigated to explain the deterioration of macroscopic mechanical properties and to elaborate the damage mechanism for future practical engineering applications.

2 Materials and experimental methods

2.1 Raw materials and mixing proportions

The cement was made of ordinary silicate cement (P·O42.5N) produced by Foshan Conch Cement Co. Ltd., and the mechanical properties of the cement are shown in Table 1. The aggregates in the concrete mix include natural coarse aggregate (NCA), RCA, and natural FA. NCA was made of crushed limestone with particle size of 5–20 mm. The RCA was produced from a demolished building in Foshan, China, with a particle size of 5–20 mm. The coarse aggregate was crushed, screened, and cleaned to comply with Chinese standards GB/T25177-2010 [32]. The appearance and particle gradation of coarse aggregate are shown in Figures 1 and 2. Natural FA is medium sand with a fineness modulus of 2.76. The basic physical indexes of NCA, RCA, and FA were tested with reference to Chinese standards GB/T14685-2011 [33] and GB/T14684-2011 [34], and their physical properties are shown in Table 2. A high-efficiency polycarboxylic acid water reducing agent was used as admixture.

In this study, the presaturation method [35–38] was referred for the design of the RAC ratio, and the ratio is shown in Table 3. The mixture was compensated with saturated RCA to offset the moisture absorbed by RCA. In this study, five concrete mixes were designed with 0, 20, 40, 60, 80, and 100% replacement rates, which were labeled as RAC-0, RAC-20, RAC-40, RAC-60, RAC-80, and RAC-100, using RCA replacement rate as the main parameter and choosing w/c = 0.5.

Table 1: Mechanical properties of Portland cement

Flexural strength (MPa)		Compressive strength (MPa)		Fineness	Setting time (min)	
3 days	28 days	3 days	28 days	1.2	Initial setting	Final setting
4.0	7.2	20.4	43.5		174	269

2.2 Specimen casting and curing conditions

According to Chinese standards GB/T50476-2008 [38], 60 groups of cubic specimens with dimensions of 100 mm × 100 mm × 100 mm (180 pieces) were designed and fabricated, with three pieces in each group. After 24 h of casting, the specimens were demolded and maintained in a standard maintenance room at 20 ± 2°C and 95%

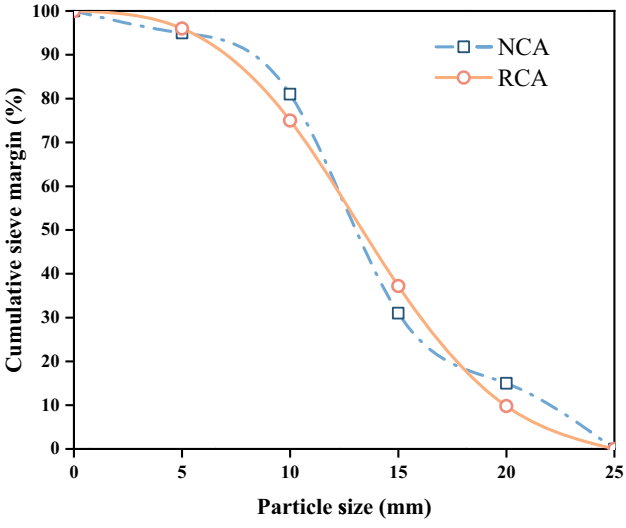

Figure 1: Particle gradation of coarse aggregates.

(a) (b)

Figure 2: Appearance of coarse aggregates: (a) NCA and (b) RCA.

relative humidity for 24 days. For 24 days, the specimens were immersed in a solution of sodium chloride with a mass fraction of 3.5% for 4 days. The finished specimens were used for cubic compressive strength test, mass loss test, and elastic modulus test, respectively.

2.3 Experimental methods

2.3.1 Salt-frost cycles test

According to the fast freezing method in Chinese standards GB/T 50082-2009 [40], the salt-frost cycles test was carried out using a rapid freeze–thaw testing machine for concrete with model number TDR-10. The number of salt-frost cycles were 0, 25, 50, 75, and 100, and the test procedure is shown in Figure 3.

2.3.2 Dynamic modulus of elasticity and mass loss tests

To obtain data on the RDME, this study used the HMP-13 bdynamic elastometer to nondestructively test the dynamic modulus of elasticity of the collected specimens. The RDME of concrete was determined by equation (1).

Table 3: Mix proportion of RAC (kg·m^{-3})

Specimens	Water	Cement	Sand	NCA	RCA	SP
RAC-0	189	378	712	1162.2	0	1.9
RAC-20	189	378	712	929.8	232.4	1.9
RAC-40	189	378	712	697.3	464.9	1.9
RAC-60	189	378	712	464.9	697.3	1.9
RAC-80	189	378	712	232.4	928.8	1.9
RAC-100	189	378	712	0	1162.2	1.9

$$p_i = \frac{f_{ni}^2}{f_{0i}^2} \times 100\%, \tag{1}$$

p_i is the RDME (%) of the ith concrete specimen after N freeze–thaw cycles, f_{ni} is the transverse fundamental frequency (Hz) of the ith concrete specimen after N freeze–thaw cycles, and f_{0i} is the initial value of transverse fundamental frequency (Hz) of the ith concrete specimen before the freeze–thaw cycle test.

The specimens were removed from the brine with different number of salt-frost cycles and dried the surface water, and their MLR was determined, and the MLR was determined by equation (2).

$$\Delta m_{ni} = \frac{m_{0i} - m_{ni}}{m_{0i}} \times 100\%, \tag{2}$$

Δm_{ni} is the MLR (%) of the ith concrete specimen after N freeze–thaw cycles, m_{0i} is the mass (g) of the ith concrete specimen before the freeze–thaw cycles test, and m_{ni} is the mass (g) of the ith concrete specimen after N freeze–thaw cycles.

2.3.3 Compressive strength test

According to Chinese standards GB/T50081-2019 [41], an electro-hydraulic pressure tester of model NYL was used to test the compressive strength of the specimens under different salt-frost cycles. All test specimens were grouped in groups of three, and the arithmetic mean of their measured values was taken as the final result.

Table 2: Physical properties of aggregates

Physical properties	Coarse aggregate		FA
Type	Natural stone	Recycle stone	Natural sand
Bulk density (kg·m^{-3})	1,650	1,450	2,050
Apparent density (kg·m^{-3})	2,550	2,360	2,512
Water content (%)	0.12	2.51	0.81
Mass water absorption (%)	1.21	12	7.58
Crushing value (%)	5.32	27.6	—

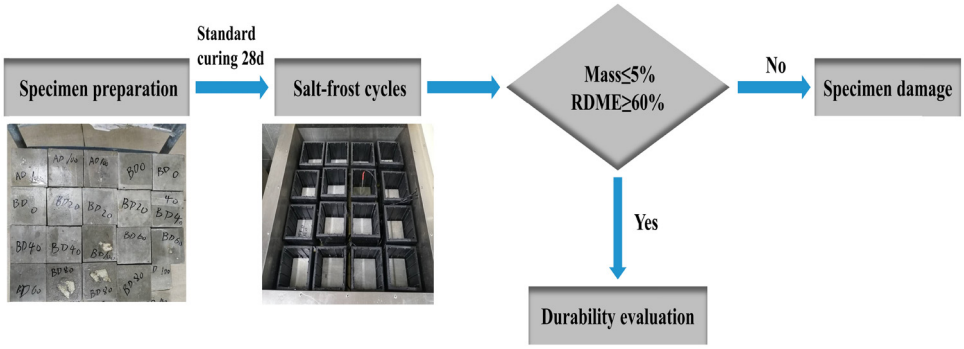

Figure 3: Test flow chart of salt-frost cycles.

2.3.4 Material properties testing

To further investigate the effect of RCA on the freezing and corrosion disturbance of recycled concrete under the action of salt-frost cycles, the microscopic morphology, pore structure distribution, enhancement mechanism, and damage characteristics of hydration products and chemical bonds or molecules of recycled concrete specimens under different numbers of salt-frost cycles were analyzed using scanning electron microscopy (SEM), Fourier-transform infrared spectroscopy (FTIR), and mercury-pressure porosimetry (MIP). For microscopic performance, the test procedures were as follows. First, the specimens that reached the number of salt-freezing cycles were broken into 2–5 mm pellets. Second, these pellets were immersed in alcohol for 24 h to terminate the reaction. Then, the pellets were dried at 60°C for 48 h. Finally, the treated pellets were stored in a desiccator. The specimens were sprayed with gold and subjected to SEM analysis. The pellets were ground together with potassium bromide and pressed into thin slices for FTIR analysis. In addition, samples of 0.5–1 g were weighed and put into swellers, sealed with vacuum grease, and then subjected to MIP analysis using low and high pressure. The drying and preparation conditions of the samples were in accordance with Chinese standards GB/T 16594-2008 [42], ISO 19618-2017 [43], and GB/T 21650-2008 [44].

3 Results and discussion

3.1 Effect of salt-frost cycles on RAC

3.1.1 Surface damage pattern of RAC specimens

Figure 4(a) shows the damage pattern of RAC-60 specimens under different number of salt-frost cycles. With the increase of the number of salt-frost cycles, the surface of the specimens become increasingly rougher. Before the salt-frost cycles, the surface of each group of specimens is flat and smooth with a dense cement mortar package. After 25N salt-frost cycles, many pits appear on the surface of the specimens due to the spalling of the surface mortar. With the further increase of the number of salt-frost cycles, holes begin to appear on the surface of the specimens and the coarse aggregate is gradually exposed. In addition, the increase of RCA would aggravate the damage of the specimens. As shown in Figure 4(b), at reaching 100N salt-frost cycles, mortar spalling and exposed coarse aggregate soon appear on the surface of the specimens with the increase of RCA content. At 60% of RCA content, the surface of the specimen have mortar completely spalled off, aggregate exposed, and the edges collapsed because the strength of the old mortar attached to the aggregate is lower than that of the new mortar. Therefore, it is less sensitive to the osmotic pressure and resistance to crystallization pressure induced by salt-frost cycles than natural coarse concrete (NC) samples, leading to further damage. This result is similar to that reported by many researchers [45–47].

3.1.2 RDME and mass loss of RAC

The results of dynamic modulus of elasticity of RAC for different number of salt-frost cycles are shown in Figure 5. With the increase of the number of salt-frost cycles, the RDME of the RAC decreases more than that of the normal concrete. After 75N salt-frost cycles, the RDME of RAC-100 specimens decreases to 57.6%, which is lower than the critical value of RDME (60%). Meanwhile, the salt-frost cycles is more likely to negatively affect the RDME of the RAC compares with the normal concrete. 25N salt-frost cycles of the RAC specimens show a severe loss of RDME. In the final stage, the loss of RDME is significantly reduced. In addition,

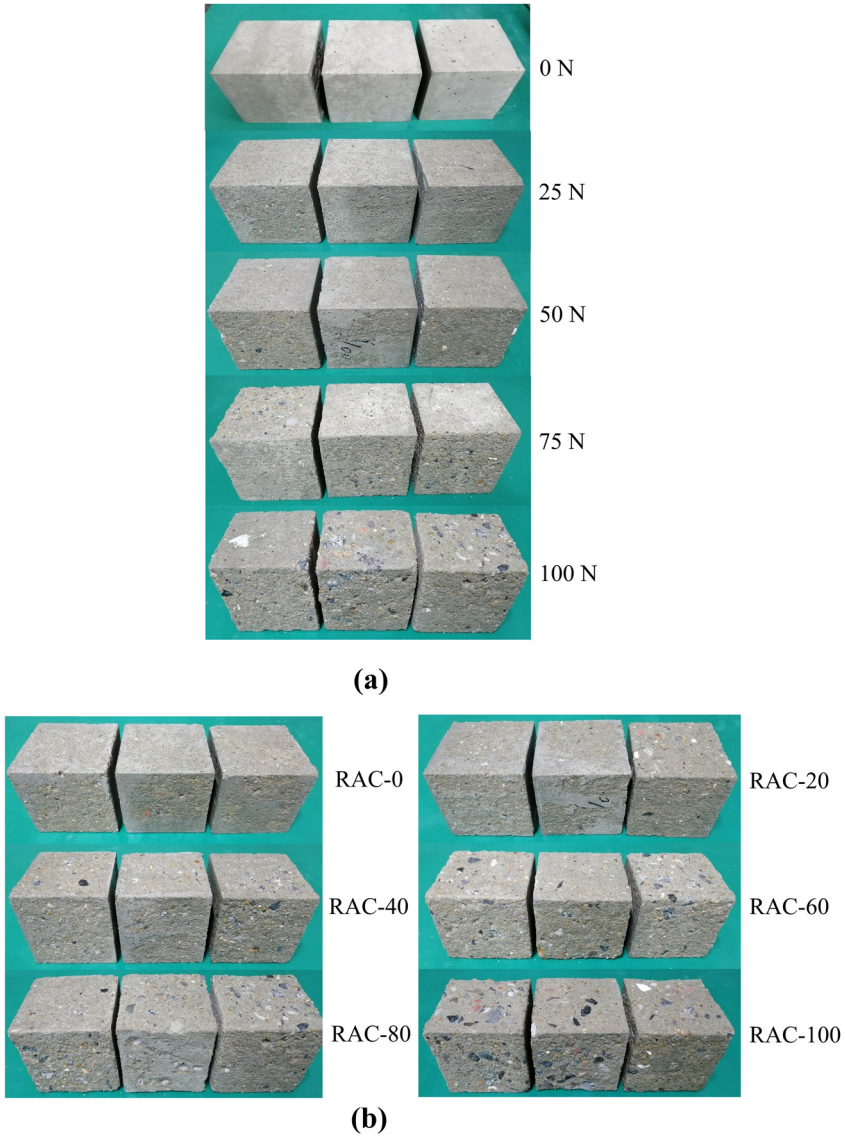

Figure 4: Damage morphology of specimens after salt-frost cycles: (a) RAC-60 and (b) 100N.

the incorporation of RCA contributes to produce a more significant reduction in RDME of RAC. This may be attributed to the poor bonding of the old mortar to the new mortar on the RCA surface, which is more prone to internal cracking under crystallization pressure, resulting in a reduction in RDME.

The MLR of RAC under different number of salt-frost cycles is shown in Figure 6. For the RAC specimens with less than 40% RCA admixture, the MLR of RAC only changes by about 0.4% under 25N salt-frost cycles. This may be due to the presence of brine crystals in the internal pores of the concrete, which offset part of the spalling of the cement mortar. The MLR of the concrete gradually increases with the number of salt-frost cycles. Similarly, the incorporation of RCA intensifies the deterioration of the concrete specimens. Specimens of RAC-80 and RAC-100 are elevated to 5.1 and 6.8% mass loss after 100N salt-frost cycles, which exceed the MLR threshold (5%). As analyzed by Zhu et al. [48], the mass change of concrete under freeze–thaw cycles is the result of a combination of water intrusion mass increase and surface scaling mass loss. When the number of salt-frost cycles is low, the specimens have less freeze damage, and the mass gained by the specimens from solution crystallization can mitigate mass loss due to spalling. With the increase of the number of salt-frost cycles and RCA content, the frost damage of the specimens becomes more and more serious, the cracks increase, the aggregate and mortar fall off, and the mass gain from solution crystallization is smaller than

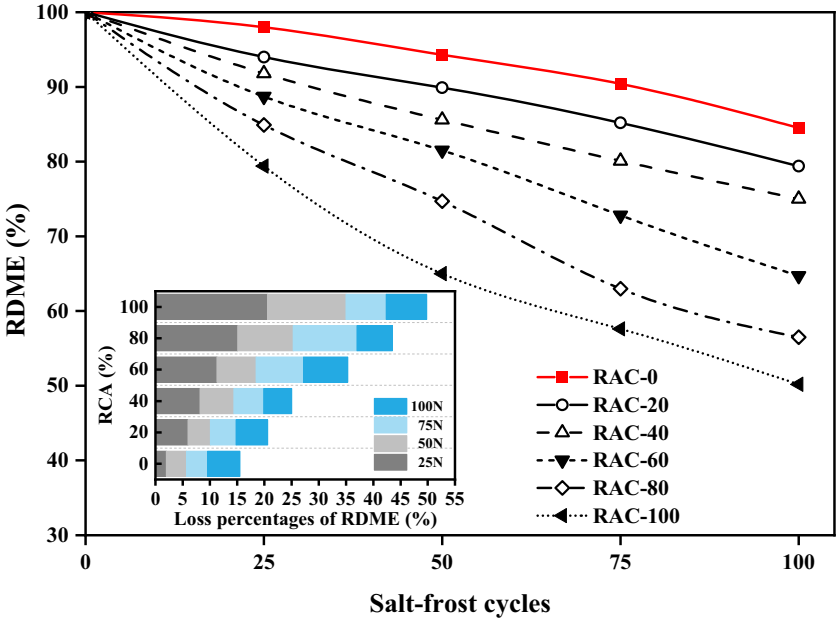

Figure 5: The RDME of concrete after salt-frost cycles.

the mass loss from specimen spalling, which leads to a substantial loss of the overall mass of the specimens.

3.1.3 Changes in compressive strength of RAC

Figure 7 shows the change law of compressive strength of RAC under different number of salt-frost cycles. It can be seen that the compressive strength of RAC decreases with the increase of the number of salt-frost cycles and the amount of RCA content. After more than 75N salt-frost cycles, the compressive strength loss of RAC-0, RAC-20, and RAC-40 is relatively moderate, whereas the compressive strength loss of RAC-60, RAC-80, and RAC-100 increase steeply, and their strength loss rates reach 20, 21.9, and 17.5%, respectively. This indicates that the large amount

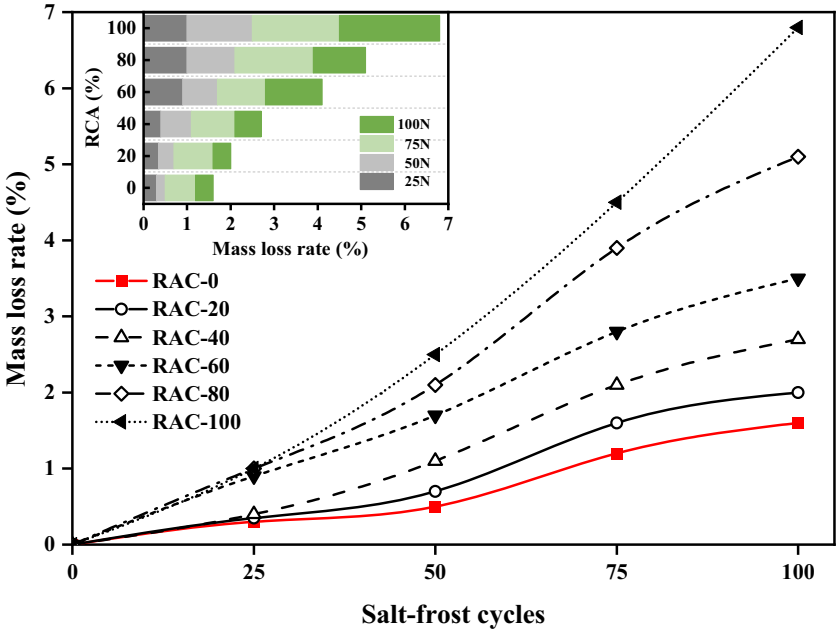

Figure 6: The MLR of concrete after salt-frost cycles.

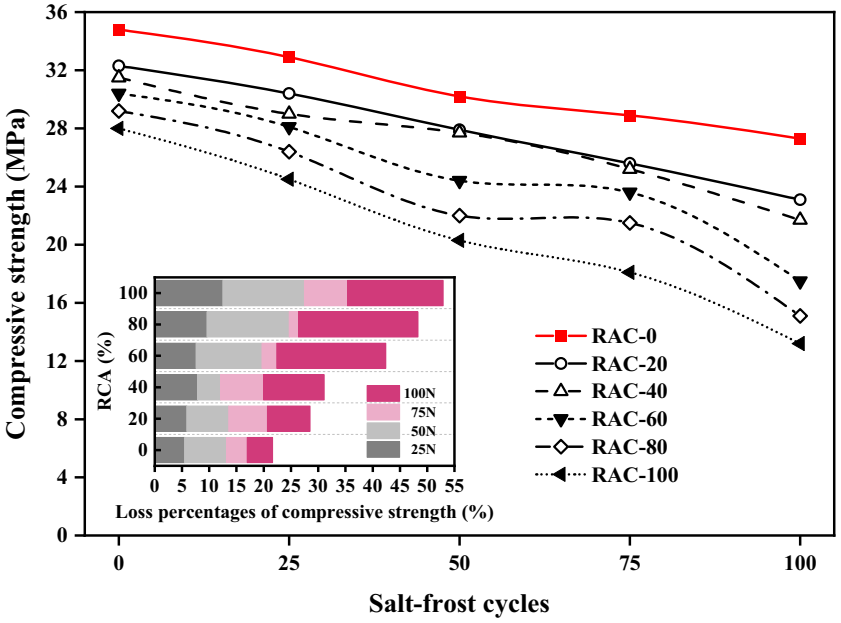

Figure 7: The compressive strength of concrete after salt-frost cycles.

of RCA is very detrimental to RAC at the late stage of salt-frost cycles. The reason is that the number of original microcracks of RCA is high and the bond between the old mortar and the aggregate or the old mortar and the new mortar is poor, which leads to the high frost swelling force generated during the salt-frost cycles. At the same time, the NaCl crystals are formed by the salt entering the concrete interior with the cracks further strengthen the extrusion and swelling damage to the internal capillaries and microcracks of the concrete, which severely damages its internal structure; however, the crushing index and the needle-like content of the RCA are greater than those of the natural aggregate, which also leads to a lower strength of RAC than ordinary concrete and an increased rate of compressive strength loss after the salt-frost cycles [49].

3.2 Material properties of RAC after salt-frost cycles

3.2.1 Material morphology changes of RAC

The microscopic morphological changes of the materials under 0N and 100N salt-frost cycles are determined by SEM for RAC-0, RAC-40, and RAC-100, as shown in Figure 8. It can be seen that all the concrete internal structures are relatively dense in the initial state, with only a few micropores and microcracks. However, the interface transition zone (ITZ) of conventional concrete is more compact than RAC-100, which is due to the old mortar attached to the surface of RCA. After 100N salt-frost cycles, the cement matrix is extruded to form wider cracks and poorer pore structure. With the increase of RCA admixture, the micropores develop into large pore size holes, and the microcracks gradually develop into cracks, showing a loose porous state. Meanwhile, the loose internal structure makes the poorly bonded ITZ further deteriorated. The results clearly show that the degradation of RAC under the coupling action of RCA and salt freezing is more severe than that under the action of single factor, which is attributed to the increase of pore size and microcracks during freeze–thawing. These pores and microcracks provide more pathways for subsequent chloride ion infiltration and promote structural damage, which leads to more severe deterioration of the complex environment.

3.2.2 Pore structure distribution of RAC

Figure 9(a) and Table 4 show the pore size distribution, porosity, total pore volume, and total pore area of RAC under different salt-frost cycles. At 0N, the curve of RAC shift significantly upward with the incorporation of RCA and the porosity increased, and the porosity of RAC-100 increased by 45.1% compares with that of RAC-0. This indicates that RCA has a negative effect on the pore structure of concrete. As the number of salt-frost cycles increased, the cumulative damage of salt-frost cycles and the collapse and blockage of some large pores eventually lead to the deterioration of the pore structure and densification inside the concrete. The

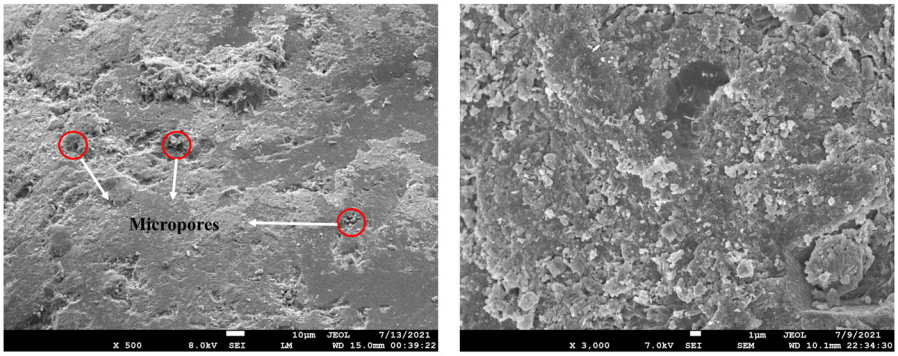

(a)

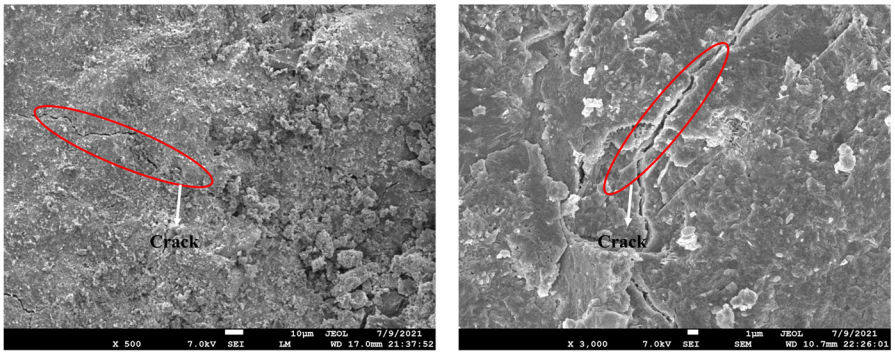

(b)

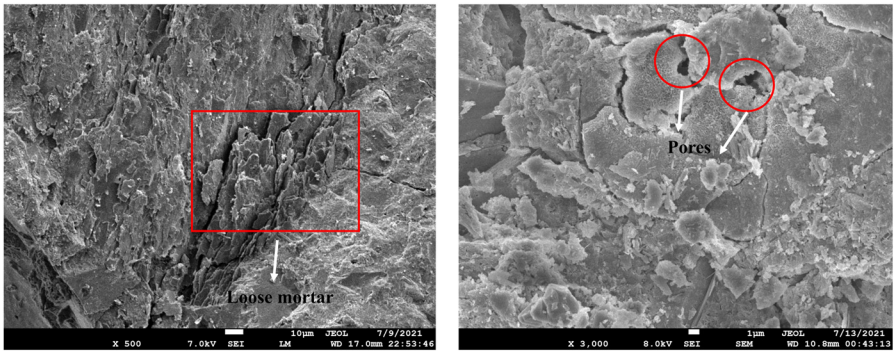

(c)

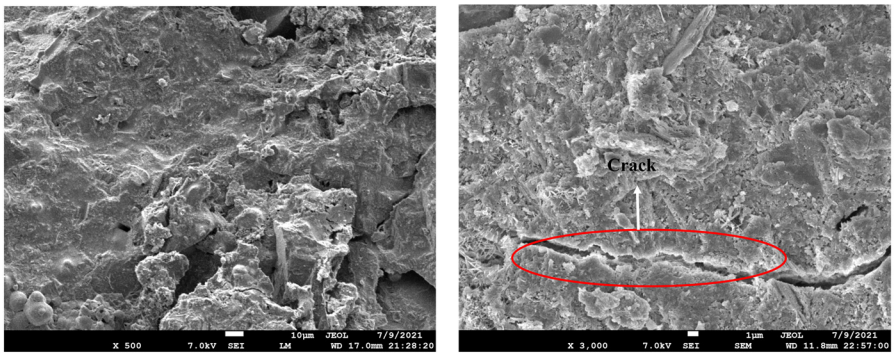

(d)

porosity of RAC-100-100N reach 26.5%, which is 134.5% higher than that of RAC-0-0N. The cumulative pore volume percentages are shown in Figure 10(b). The cumulative pore volume percentages are classified according to the principles of harmless pores (<20 nm), less harmful pores (20–100 nm), harmful pores (100–1,000 nm) and very harmful pores

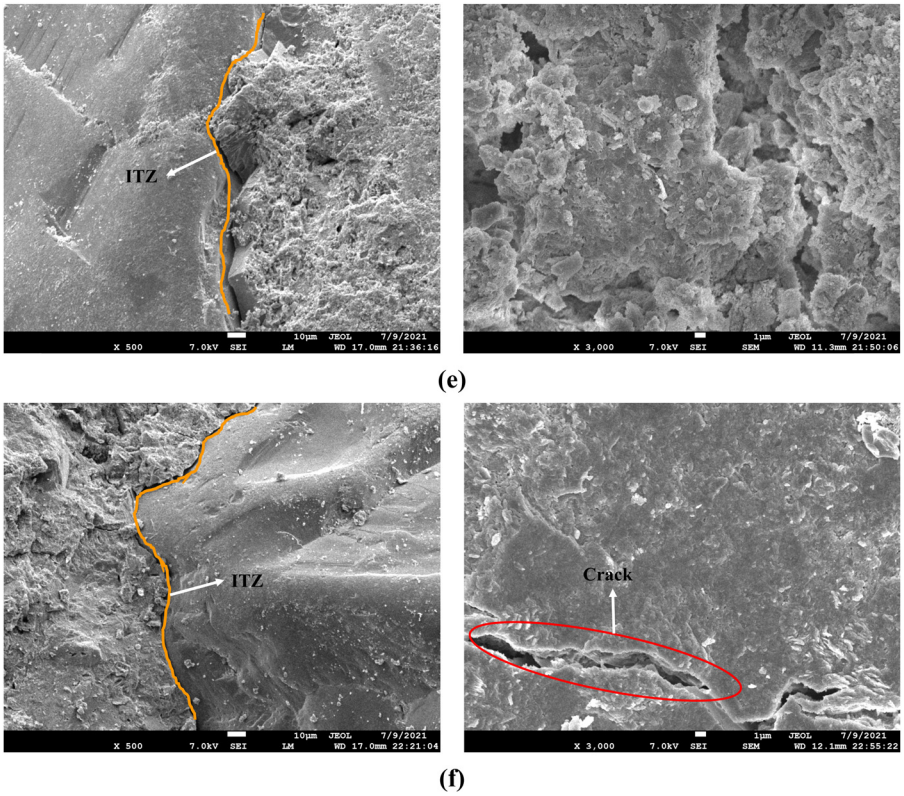

Figure 8: Micromorphology of the RAC: (a) RAC-0-0N, (b) RAC-0-100N, (c) RAC-40-0N, (d) RAC-40-100N, (e) RAC-100-0N, and (f) RAC-100-100N.

(>1,000 nm). The salt-frost cycles can significantly increase the volume fraction of harmful pores (100–1,000 nm) and decrease the volume fraction of less harmful pores (20–100 nm). In summary, the salt-frost cycling effect accelerates the degradation of RAC. This result is attributed to the fact that RCA itself has certain pores, and when the material is in the process of salt-frost cycling, the space in the pore structure is favorable for the migration of water molecules to the interior and promotes the development of ice crystals. Under hydrostatic pressure the pores are opened up to each other and large pores are formed [50].

3.2.3 Functional group changes of RAC

The changes in the functional groups of the RAC during the salt-frost cycles are determined based on FTIR and are shown in Figure 10. With the increase of the number of salt-frost cycles, the intensity of the contraction vibration of the H–O–H functional group (3,400) increased, and the expansion of the internal space lead to the extrusion and bending of water molecules raising the degree of aqueous phase deformation. In addition, the contraction vibration of Si–O functional group (970) in Q_2 tetrahedra is obvious, indicating that the enhanced polymerization of this functional group produces absorption peaks [51–53]. Meanwhile, the incorporation of RCA makes the absorption peak of the –OH functional group (3,640) weaker, which affects the proportion of functional group –OH in CH [54,55]. In conclusion, the salt-frost cycles and the incorporation of recycled aggregates affect the Si–O and –OH groups of the concrete materials, thus altering their mechanical and durability properties.

3.2.4 Damage mechanism of RAC

In this study, a large amount of mortar spalling and exposed aggregates are observed on the surface of the RAC specimens after 100N salt-frost cycles. However, the internal crack width of the concrete increased, the number of holes increases, and the ITZ is weak. However, no significant changes are observed in the plain concrete specimens after 100N salt-frost cycles. According to a previous study [56], the damage to the

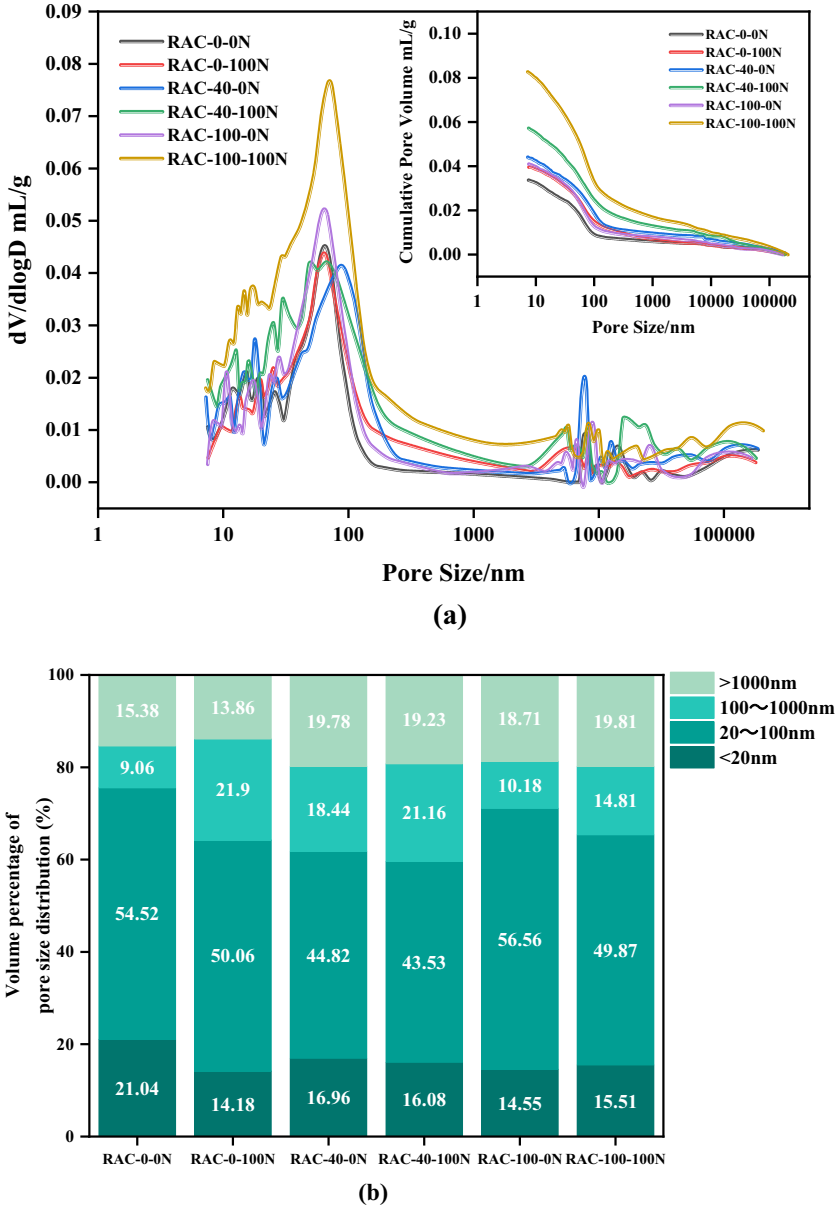

Figure 9: Pore structure distribution of RC for after salt-frost cycles: (a) pore size distribution; (b) cumulative pore volume percentage.

Table 4: Porosity, total pore size, and area of RAC

Specimen	Porosity (%)	Total intruded volume ($mL \cdot g^{-1}$)	Total surface area ($m^2 \cdot g^{-1}$)
RAC-0-0N	11.3	0.0339	3.7807
RAC-0-100N	13.6	0.0398	3.5640
RAC-40-0N	14.9	0.0442	4.1532
RAC-40-100N	18.8	0.0576	5.5077
RAC-100-0N	16.4	0.0410	3.8949
RAC-100-100N	26.5	0.0828	7.7558

internal structure of concrete exposes to salt-frost cycles may be due to water migration and crystallization expansion resulting in water pressure and frost swelling pressure. The frost swelling pressure may accelerate the development of microcracks and macrocracks when the tensile strength of concrete that can withstand is exceeded. As shown in Figure 11, as salt-frost erosion proceeds, the ITZ around the RCA is gradually filled with salt solution and further expansion of the crystals can lead to separation of the old mortar from the aggregate or the old mortar from the new mortar. Therefore, after 100N salt-frost cycles, large holes and exposed RCA appear on the

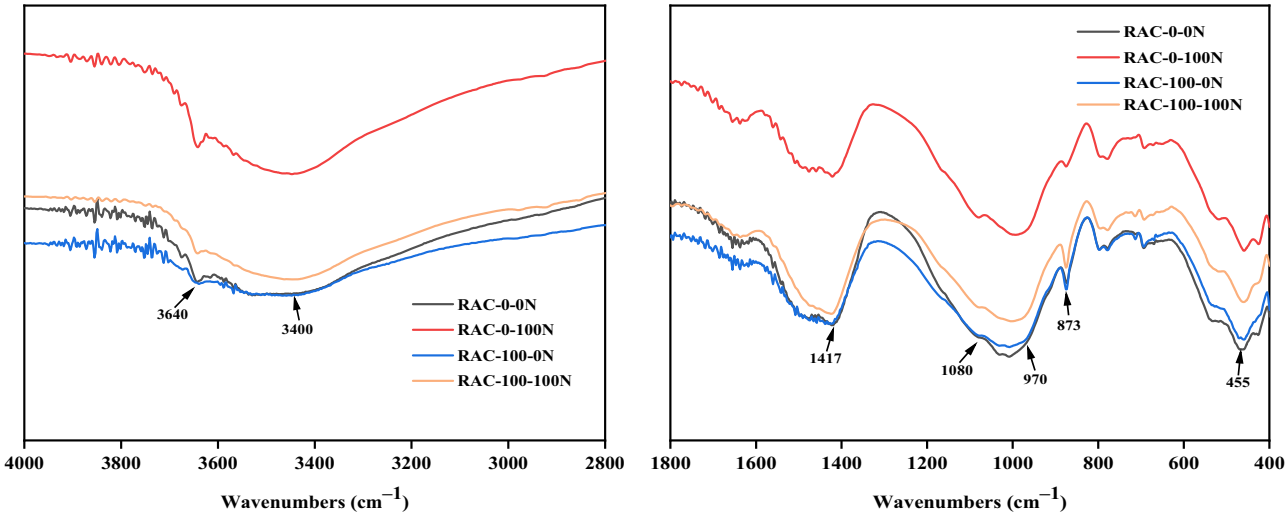

Figure 10: Function groups analysis on RAC subjected to salt-frost cycles.

surface of the specimens. This indicates that the ITZ between the RCA and the old mortar is the weak link. Compared with the RAC with multi-interface structure, the tensile strength of the ITZ with internal structure of NC is higher than that of the old ITZ. Also, the NC samples have lower porosity than the RAC samples, which limits the frost swelling due to internal pressure. Therefore, RAC is more sensitive to salt-frost cycles than natural aggregate concrete. Therefore, the use of RAC in cold coastal areas must be considered in concert to reduce the damage caused by salt-frost cycles.

4 Conclusion

This study analyzed the mechanism of the effect of salt-frost cycles on RAC based on the results of the study on

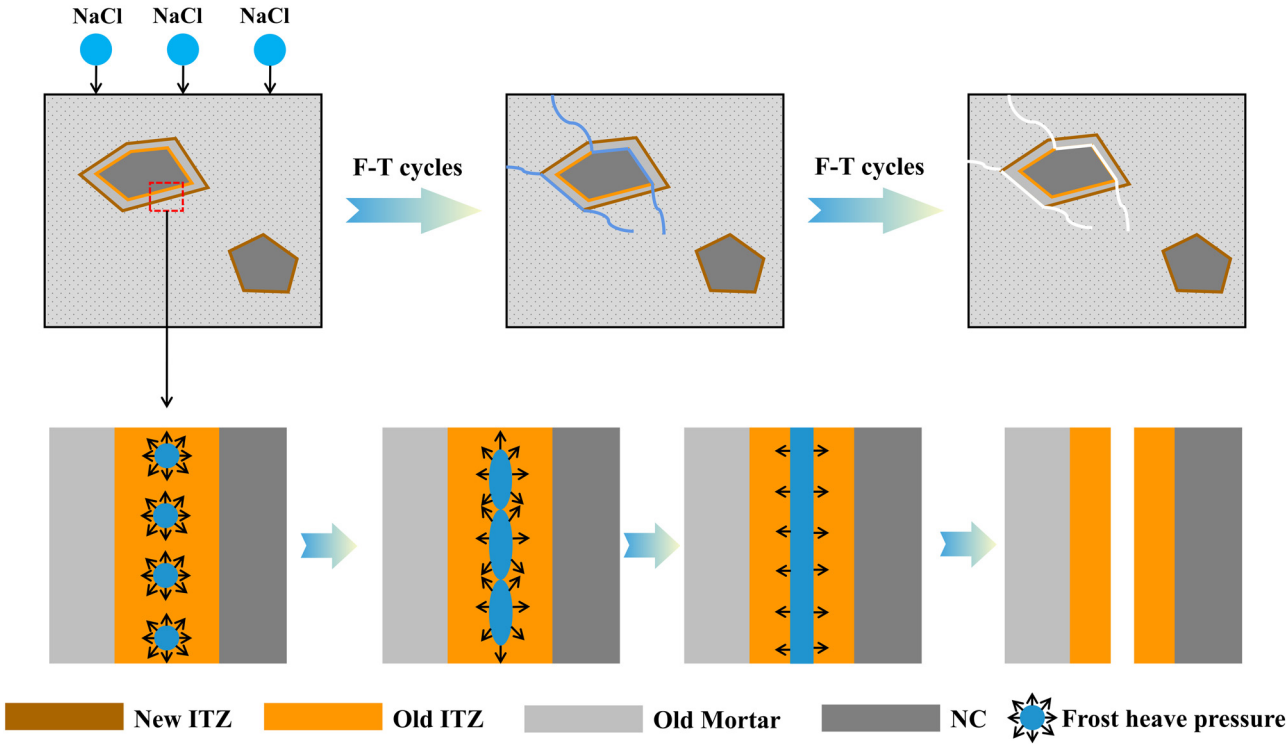

Figure 11: Damage mechanism of salt-frost cycles on RAC.

the effect of RAC performance under salt-frost cycles conditions, and concludes as follows:

(1) The incorporation of RCA accelerates the spalling of concrete under salt-frost cycles conditions. After 100 salt-frost cycles, a large number of holes and exposed aggregates appear in RAC-100 specimens.
(2) The relative dynamic modulus, MLR, and compressive strength decrease with the increase of the number of salt-frost cycles. The RDME of RAC-100 specimens is lower than 60% after 100N salt-frost cycles, and the mass loss is more than 5%. The compressive strength of specimens with more than 60% RCA admixture decreases significantly, and the compressive strength of RAC-100 after 100 salt-frost cycles is lower than that of RAC-0 by 51.6%.
(3) The damage of specimens caused by salt-frost cycles is different from that of ordinary concrete. The main damage location tend to occur in the ITZ of old mortar and coarse aggregate or old mortar and new mortar, and then the cracks extend along the surface of old mortar. Moreover, the deterioration of pore size and the effect on Si–O and –OH groups caused by salt-frost cycles are factors that cannot be ignored in reducing their mechanical and durability properties.

Acknowledgements: The authors thank the team members from ASIM Group, China, the support from Foshan Intelligent Land and Ocean Engineering Materials Engineering Technology Research and Development Center, Foshan, China.

Funding information: The Science and Technology Innovation Platform of Foshan City (Grant No. 2016AG100341, Guangdong Province, China). 2021 Guangdong Provincial Department of Education, Guangdong University Scientific Research Project-Special Project for Young Innovative Talents (2021KQNCX083)

Author contributions: Ying Yu: formal analysis, writing – original draft, and project administration; Ben Li: conceptualization – ideas, funding acquisition, and resources; Chen Zhang: investigation and visualization; and Yu Zhang: investigation and software.

Conflict of interest: We declare that we have no financial and personal relationships with other people or organizations that can inappropriately influence our work, there is no professional or other personal interest of any nature or kind in any product, service, and/or company that could be construed as influencing the position presented in, or the review of, the manuscript entitled, "Deterioration characteristics of recycled aggregate concrete under the effect of salt-frost cycles."

Data availability statement: Data available on request due to restrictions, for example, privacy or ethical.

References

[1] Li, W. G., Z. Y. Luo, C. Long, C. Q. Wu, W. H. Duan, and S. P. Shah. Effects of nanoparticle on the dynamic behaviors of recycled aggregate concrete under impact loading. *Materials & Design*, Vol. 112, 2016, pp. 58–66.
[2] Radonjanin, V., M. Malešev, S. Marinković, and A. E. S. Al Malty. Green recycled aggregate concrete. *Construction and Building Materials*, Vol. 47, 2013, pp. 1503–1511.
[3] Xiao, J., W. Li, Y. Fan, and X. Huang. An overview of study on recycled aggregate concrete in China (1996–2011). *Construction and Building Materials*, Vol. 31, 2012, pp. 364–383.
[4] Liu, J., Z. Hua, Y. Pang, and X. Wang. Risk sharing for PPP project in construction waste recycling industry in China. *Environmental Science and Pollution Research*, Vol. 29, 2021, pp. 1–15.
[5] Lu, N., S. Feng, and H. Lu. Te tempo-spatial difference of urbanization on construction sector carbon emissions in China. *Journal of Beijing Institute of Technology* (*Social Sciences Edition*), Vol. 20, 2018, pp. 8–17 (in Chinese).
[6] National Bureau of Statistics Net, Beijing, China. http://www.stats.gov.cn/.
[7] Xiao, J., Z. Ma, T. Sui, A. Akbarnezhad, and Z. Duan. Mechanical properties of concrete mixed with recycled powder produced from construction and demolition waste. *Journal of Cleaner Production*, Vol. 188, 2018, pp. 720–731.
[8] Chinese Know Net, Tsinghua University, Beijing, China. http://www.cnki.net/.
[9] Mercader-Moyano, P. and A. Ramırez-de-Arellano-Agudo. Selective classification and quantification model of C&D waste from material resources consumed in residential building construction. *Waste Management and Research*, Vol. 31, No. 5, 2013, pp. 458–474.
[10] Seror, N., S. Hareli, and B.A. Portnov. Evaluating the effect of vehicle impoundment policy on illegal construction and demolition waste dumping: Israel as a case study. *Waste Management*, Vol. 34, No. 8, 2014, pp. 1436–1445.
[11] Gálvez-Martos, J.-L., D. Styles, H. Schoenberger, and B. Zeschmar-Lahl. Construction and demolition waste best management practice in Europe. *Resources, Conservation And Recycling*, Vol. 136, 2018, pp. 166–178.
[12] Zhang, J., J. Wang, X. Li, T. Zhou, and Y. Guo. Rapid-hardening controlled low strength materials made of recycled fine aggregate from construction anddemolition waste. *Construction and Building Materials*, Vol. 173, 2018, pp. 81–89.
[13] Velay-Lizancos, M., P. Vazquez-Burgo, D. Restrepo, and I. Martinez-Lage. Effect of fine and coarse recycled concrete

aggregate on the mechanical behavior of precast reinforced beams: comparison of FE simulations, theoretical, and experimental results on real scale beams. *Construction and Building Materials*, Vol. 191, 2018, pp. 1109–1119.
[14] Xiao, J., D. Lu, and J. Ying. Durability of recycled aggregate concrete: an overview. *Journal of Advanced Concrete Technology*, Vol. 11, No. 12, 2013, pp. 347–359.
[15] Xiao, J., D. Lu, and J. Ying. Durability of recycled aggregate concrete-a review. *Cement and Concrete Composites*, Vol. 89, 2018, pp. 251–259.
[16] Evangelista, L. and J. De Brito. Durability performance of concrete made with fine recycled concrete aggregates. *Cement and Concrete Composites*, Vol. 32, No. 1, 2010, pp. 9–14.
[17] Chen, H., Z. Peng, W. Zeng, and J. Wu. Salt movement during soil freezing events in inner Mongolia, China. *Journal of Coastal Research*, Vol. 82, No. 10082, 2018, pp. 55–63.
[18] Yi J., Comprehensive experimental study of compressive and anti-chloride ion erosion ability of recycled high performance concrete. *Journal of Shijiazhuang Institute of Railway Technology*, Vol. 13, 2014, pp. 81–86 (in Chinese).
[19] Ye, T., Y. Xu, and J. Zhang. Experimental study on chloride penetration resistance performance of recycled concrete. *Journal of Changchun University of Technology* (*Natural Science Edition*), Vol. 35, No. 5, 2014, pp. 567–571 (in Chinese).
[20] Han, S., Q. Y. Li, G. B. Yue, J. Mo, and X. F. Wang. Influence of quality and substitution rate of recycled coarse aggregate on coefficient of the chloride migration of recycled concrete. *Concrete*, Vol. 314, No. 12, 2015, pp. 80–83 (in Chinese).
[21] Qin, H. and H. Tang. Experimental study on influence of coarse aggregate content on chloride penetration resistance of recycled aggregate concrete. *Journal of China and Foreign Highway*, Vol. 35, No. 6, 2015, pp. 286–290 (in Chinese).
[22] Ouyang, Z. and Y. Chen. Study on chloride permeability of recycled concrete after repeated compressive stress. *Concrete*, Vol. 327, No. 1, 2017, pp. 31–33 (in Chinese).
[23] Adessina, A., A. B. Fraj, J. F. Barthélémy, C. Chateau, and D. Garnier. Experimental and micromechanical investigation on the mechanical and durability properties of recycled aggregates concrete. *Cement and Concrete Research*, Vol. 126, 2019, id. 105900.
[24] Abbas, A., G. Fathifazl, O. B. Isgor, A. G. Razaqpur, B. Fournier, and S. Foo. Durability of recycled aggregate concrete designed with equivalent mortar volume method. *Cement and Concrete Composites*, Vol. 31, 2009, pp. 555–563.
[25] Yildirim, S. T., C. Meyer, and S. Herfellner. Effects of internal curing on the strength, drying shrinkage and freeze-thaw resistance of concrete containing recycled concrete aggregate. *Construction and Building Materials*, Vol. 91, 2015, pp. 288–296.
[26] Bogas, J. A., J. Brito, and D. Ramos. Freeze-thaw resistance of concrete produced with fine recycled concrete aggregates. *Journal of Cleaner Production*, Vol. 115, 2016, pp. 294–306.
[27] Huda, S. B. and M. S. Alam. Mechanical and freeze-thaw durability properties of recycled aggregate concrete made with recycled coarse aggregate. *Journal of Materials in Civil Engineering*, Vol. 27, No. 10, 2015, id. 04015003.
[28] Vázquez, E., M. Barra, D. Aponte, C. Jiménez, and S. Valls. Improvement of the durability of concrete with recycled aggregates in chloride exposed environment. *Construction and Building Materials*, Vol. 67, Part A, 2014, pp. 61–67.
[29] Ying, J., J. Xiao, and V. W. Tam. On the variability of chloride diffusion in modelled recycled aggregate concrete. *Construction and Building Materials*, Vol. 41, 2013, pp. 732–741.
[30] Hu, B., S. Zheng, and G. Ren. The experimental study on the frost resistance of different recycled coarse aggregate replacement rate of recycled concrete. *DEStech Transactions on Materials Science and Engineering*, Vol. 15816, 2017, pp. 21–37.
[31] Mehta, P. K. Durability-critical issues for the future. *Concrete International*, Vol. 20, No. 7, 1997, pp. 27–33.
[32] GB/T 25177-2010. Regenerated coarse aggregate for concrete, Ministry of Housing and Urban-Rural Construction of the People's Republic of China, 2010.
[33] GB/T 14685-2011. Construction pebbles and gravels, China Federation of Building Materials, 2011.
[34] GB/T 14684-2001. Construction Sand, State Bureau of Construction Materials Industry, 2001.
[35] Wang, Q., Y. Wang, G. Yue, and Z. Huan. Influence of mixing methods on mechanical behaviors of recycled aggregate concrete. *Journal of Building Structure*, Vol. 37, No. s2, 2016, pp. 79–87 (in Chinese).
[36] Yildirim, S. T., C. Meyer, and S. Herfellner. Effects of internal curing on the strength, drying shrinkage and freeze-thaw resistance of concrete containing recycled concrete aggregates. *Construction and Building Materials*, Vol. 91, 2015, pp. 288–296.
[37] Richardson, A., K. Coventry, and J. Bacon. Freeze/thaw durability of concrete with recycled demolition aggregate compared to virgin aggregate concrete. *Journal of Cleaner Production*, Vol. 19, No. 2–3, 2011, pp. 272–277.
[38] Xuan, D., B. Zhan, and C. S. Poon. Assessment of mechanical properties of concrete incorporating carbonated recycled concrete aggregates. *Cement and Concrete Composites*, Vol. 65, 2016, pp. 67–74.
[39] GB/T 50476-2008. Design Specification for Durability of Concrete Structures, China, 2009.
[40] GB/T 50082-2009. Standard for Testing Methods for Long-Term and Durability of Common Concrete, China, 2009.
[41] GB/T 50081-2019. Standard for Testing Methods of Mechanical Properties of Normal Concrete, China, 2019.
[42] GB/T 16594-2008. General Rules for Measurement of Length in Micron Scale by SEM, ISO, Geneva, Switzerland, 2008.
[43] ISO 19618-2017. Measurement Method for Normal Spectral Emissivity Using Blackbody Reference with an FTIR Spectrometer, ISO, Geneva, Switzerland, 2017.
[44] GB/T 21650-2008. Pore Size Distribution and Porosity of Solid Materials by Mercury Porosimetry and Gas adsorption. Part 1: Mercury Porosimetry, ISO, Geneva, Switzerland, 2008.
[45] Powers, T. C. A working hypothesis for further studies of frost resistance of concrete. *ACI Journal Proceedings*, Vol. 16, No. 4, 1945, pp. 245–272.
[46] Álava, H. E., E. Tsangouri, N. De Belie, and G. De Schutter. Chloride interaction with concretes subjected to a permanent splitting tensile stress level of 65%. *Construction and Building Materials*, Vol. 127, 2016, pp. 527–538.
[47] Powers, T. C. and R. A. Helmuth. Theory of volume changes in hardened Portland cement paste during freezing. *Proceedings of Highway Research Board*, Vol. 32, 1953, pp. 285–297.
[48] Zhu, P., Y. Hao, H. Liu, X. Wang, and L. Gu. Durability evaluation of recycled aggregate concrete in a complex environment. *Journal of Cleaner Production*, Vol. 273, 2020, id. 122569.

[49] Júnior, N. A., G. A. O. Silva, and D. V. Ribeiro. Effects of the incorporation of recycled aggregate in the durability of the concrete submitted to freeze-thaw cycles. *Construction and Building Materials*, Vol. 161, 2018, pp. 723–730.
[50] Wang, Y., Z. Liu, K. Fu, Q. Li, and Y. Wang. Experimental studies on the chloride ion permeability of concrete considering the effect of freeze–thaw damage. *Construction and Building Materials*, Vol. 236, 2020, id. 117556.
[51] Richard, T., L. Mercury, F. Poulet, and L. d'Hendecourt. Diffuse reflectance infrared Fourier transform spectroscopy as a tool to characterise water in adsorption/confinement situations. *Journal of Colloid and Interface Science*, Vol. 304, No. 1, 2006, pp. 125–136.
[52] Yu, P., R. J. Kirkpatrick, B. Poe, P. F. McMillan, and X. Cong. Structure of calcium silicate hydrate (C–S–H): Near-, Mid-, and Far-infrared spectroscopy. *Journal of the American Ceramic Society*, Vol. 82, No. 3, 1999, pp. 742–748.
[53] Lodeiro, I. G., D. E. Macphee, A. Palomo, and A. Fernández-Jiménez. Effect of alkalis on fresh C-S-H gels. FTIR analysis. *Cement and Concrete Research*, Vol. 39, No. 3, 2009, pp. 147–153.
[54] Silva, D. A. D., H. R. Roman, and P. J. P. Gleize. Evidences of chemical interaction between EVA and hydrating Portland cement. *Cement and Concrete Research*, Vol. 32, No. 9, 2002, pp. 1383–1390.
[55] Ridi, F., E. Fratini, S. Milani, and P. Baglioni. Near-infrared spectroscopy investigation of the water confined in tricalcium silicate pastes. *The Journal of Physical Chemistry B*, Vol. 110, No. 33, 2006, pp. 16326–16331.
[56] Sidorova, A., E. Vazquez-Ramonich, M. Barra-Bizinotto, J. J. Roa-Rovira, and E. Jimenez-Pique. Study of the recycled aggregates nature's influence on the aggregate–cement paste interface and ITZ. *Construction and Building Materials*, Vol. 68, 2014, pp. 677–684.